# Journal of Materials Chemistry A

Accepted Manuscript


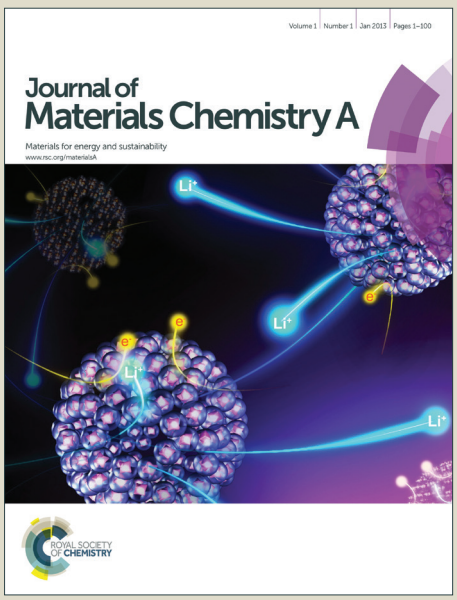





ROYAL SOCIETY OF CHEMISTRY

www.rsc.org/materialsA

Journal of Materials Chemistry A RSC

PAPER

# Porous Nitrogen-Doped Hollow Carbon Spheres Derived from Polyaniline for High Performance Supercapacitors

Jinpeng Han,[a] Guiyin Xu,[a] Bing Ding,[a] Jin Pan,[a] Hui Dou*[a] and Douglas R. MacFarlane*[b]

Porous nitrogen-doped hollow carbon spheres (PNHCS) had been prepared by pyrolysis of hollow polyaniline spheres (HPS), which were synthesized by use of sulfonated polystyrene spheres (SPS) as a hard template. The PNHCS have a specific surface area (213 $m^2$ $g^{-1}$) and pore volume (0.24 $cm^3$ $g^{-1}$). At a current density of 0.5 A $g^{-1}$, the specific capacitance of the PNHCS prepared is *ca* 213 F $g^{-1}$. Capacity retention after 5000 charge/discharge cycles at a current density of 1 A $g^{-1}$ is more than 91%. The enhanced electrochemical performance can be attributed to the unique carbon nanostructure and nitrogen-doping of the PNHCS electrodes. The hollow macro-structure plays the role of an "ion-buffering" reservoir. The micropores of the PNHCS enlarge the specific surface area, while the mesopores offer larger channels for liquid electrolyte penetration. Nitrogen groups in the PNHCS not only improve the wettability of the carbon surface, but also enhance the capacitance by addition of a pseudocapacitive redox process.

## Introduction

Currently, growing shortages of traditional energy sources and fears of greenhouse gas induced global warming are prompting scientists and engineers to develop renewable, highly efficient methods of creating and storing energy without damage to the environment.[1, 2] To meet the demands of these growing sustainable energy applications, new and environment-friendly energy storage device technologies have been a research issue for several decades. Electrochemical capacitors, also known as supercapacitors, have significant potential as energy storage devices due to their unique suite of properties, including high power density, long cyclic life, fast charge/discharge rates, and low manufacturing costs.[3, 4] According to the mechanism of charge storage, supercapacitors can be divided into two types, namely, electric double-layer capacitors (EDLCs) and pseudocapacitors.[5] EDLCs have been extensively used in portable electronic devices because of their distinctive electrical properties. Various types of carbon materials with high surface area and high electrical conductivity have been used as electrode materials in this technology, including activated carbons,[6, 7] carbon nanotubes,[8, 9] graphene,[10, 11], carbon aerogels,[12, 13], carbon spheres,[14-16] hollow carbon spheres,[17] carbon nanoparticles[18] and nitrogen-doped porous carbon foams.[19]

Compared with most pseudocapacitor electrode materials such as metal oxides and conductive polymers, carbon-based electrode materials offer lower specific capacitance and energy density in the supercapacitor application. As a result much work has been devoted to improving the electrochemical properties of carbon-based materials. Based on previous reports, heteroatoms and functional groups present in a carbon matrix can significantly change its electron/donor characteristics as an electrode material. In particular it is known that the nitrogen containing functional groups in nitrogen-enriched carbon materials can enhance the capacitance of the material by addition of redox pseudocapacitance.[20-23] The carbonization of conducting polymers, such as polypyrrole (PPY) and polyaniline (PANI), has been used to obtain such nitrogen-enriched carbon materials.[24-27] In our previous work, the preparation of nitrogen-doped carbon nanotubes (NCNT) from a tubular polypyrrole (T-PPY) was studied as an EDLC electrode material. It was found that the introduction of nitrogen improved the specific capacitance of the material, however the low specific surface area (92 $m^2$ $g^{-1}$) produced only a low specific capacitance of 180 F $g^{-1}$ at a current density of 0.5 A $g^{-1}$.[28]

On the other hand, an appropriate microstructure can improve the electrochemical performance of carbon-based electrode materials by providing high electrochemically accessible surface area. Hollow carbon materials have been recognized as one kind of promising approach in this regard.[2, 4, 29, 30] Their unique structure provides a large specific surface area along with reduced diffusion lengths for both mass and charge transport. In this paper, we describe the synthesis of

porous nitrogen-doped hollow carbon spheres (PNHCS) *via* carbonization of hollow polyaniline spheres (HPS), which were prepared by a hard template method. PANI is chosen as precursor for the PNHCS owing to the high N/C ratio (0.167) and high stability at relatively high temperatures. The pyrolysis of PANI can result in N-doped carbons with high nitrogen content.[31] We show that, as electrode materials for supercapacitors, the PNHCS exhibit high specific capacitance, excellent rate performance and good long-term cycling stability.

## Results and discussion

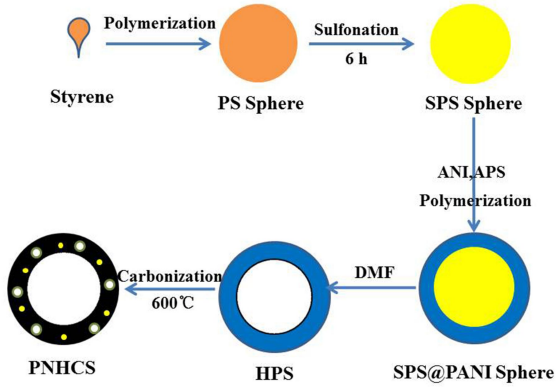


**Scheme 1.** Illustration of the synthesis route for the PNHCS.

Scheme 1 shows the synthetic procedures for the formation of PNHCS. Briefly, Polystyrene (PS) spheres prepared by standard methods are chosen as the hard template.[32] The PS spheres were added to concentrated sulfuric acid with stirring for 6 h at 40 °C to introduce sulfonic acid groups onto their surface. These sulfonic acid groups can proton transfer to the added aniline (ANI), simultaneously the strong electrostatic and hydrogen bonding forces forming a uniform aniline shell.[33] After ammonium persulphate (APS) as initiator was added, polymerization of the monomers occurs on the surface of the sulfonated PS (SPS) spheres, resulting in a SPS@PANI core-shell structure. In order to obtain the dimensional homogeneity and complete morphology of the HPS, a template removing procedure is necessary.[34] The SPS@PANI particles were dispersed into N,N-dimethylformamide (DMF) to remove the SPS core, leaving the HPS to be collected. Finally, the HPS were carbonized and annealed at 600 °C for 90 min under a nitrogen atmosphere to form the nitrogen-enriched PNHCS with uniform dimensions and complete morphology. The time and temperature for this step was based on previous work that has investigated a range of times between 60 and 120 min and temperatures between 600 to 900℃.[20, 22, 25]

The morphologies of the PNHCS were detected by scanning electron microscopy (SEM) and transmission electron microscopy (TEM). It can be seen that the SPS spheres has a uniform spherical morphology (Figure 1a). After templating and carbonization, the PNHCS maintain this spherical structure, and some damaged PNHCS observed indicate their hollow structure (Figure 1b). The TEM images further reveal the hollow sphere morphology of the PNHCS, and also confirm that the SPS spheres template is successfully removed (Figure 1c). The diameter of the PNHCS cavities and the thickness of the PNHCS shells are *ca* 550 nm and 23 nm, respectively (Figure 1d and Figure 1e). The PNHCS shell shows a highly developed microporous structure due to the pyrolysis and carbonization of the HPS (Figure 1f).

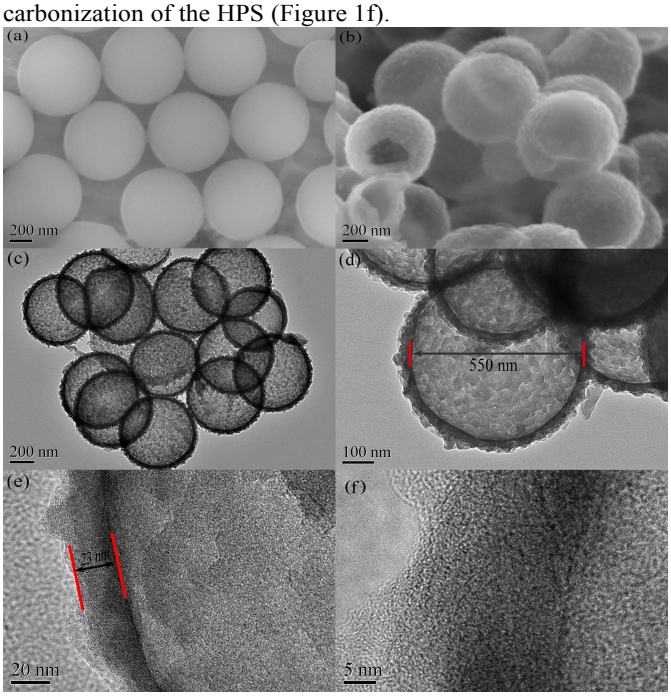


**Figure 1.** SEM images of (a) sulfonated PS spheres (b) PNHCS and (c)-(f) TEM images of PNHCS at different magnifications.

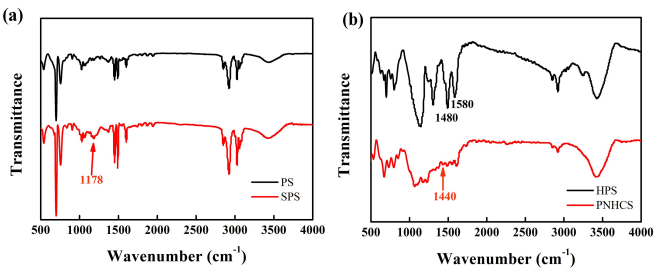


**Figure 2.** FT-IR spectra of (a) PS spheres and SPS; (b) HPS and PNHCS.

Fourier transform infrared spectrometry (FT-IR) was used to identify the functional groups of SPS, HPS and PNHCS (Figure 2). Figure 2a shows a one-to-one correspondence between the main peaks of PS and SPS. The peak at 1178 $cm^{-1}$ is related to the sulfonate group of SPS.[33] The FT-IR spectrum of HPS in Figure 2b indicates the emeraldine salt form of PANI with two characteristic peaks at 1580 $cm^{-1}$ and 1480 $cm^{-1}$ corresponding to the stretching vibration of the quinoid ring and benzenoid ring.[35] The characteristic feature of the PNHCS at 1440 $cm^{-1}$ corresponds to the C-N stretching vibration, indicating the presence of N-containing groups on the surface of the PNHCS.[36, 37]

X-ray photoelectron spectroscopy (XPS) was employed to further analyze the nature and amount of functional groups of the PNHCS. The XPS survey spectrum of the PNHCS sample with binding energies of 0-1300 eV is presented in Figure 3a.

Three peaks assignable to C1s, N1s and O1s indicate the high purity of the carbon without the presence of any undesirable compositions. Two strong peaks in the C1s spectrum (Figure 3b) located at 285.0, 286.2 eV and one minor peak at 289.5 eV are attributed to $sp^3$ C-C, C-O and −COO or O−COO carbons, respectively.[23, 38] The N1s spectrum is shown in Figure 3c. As expected, an intense peak at 398.5 eV and a small one at 403.2 eV can be distinguished, the former corresponding to the pyridinic nitrogen, and the latter to an oxidized pyridinic nitrogen. The peak at 399.9 eV can be identified as corresponding to pyrrolic-N. The peak at 399.9 eV can be identified as corresponding to pyrrolic-N. The intense peak at 401.0 eV may be attributed to quaternary-N, which is the most stable nitrogen species under pyrolysis conditions.[20, 21, 39] Figure 3d shows the different nitrogen-doping forms in the PNHCS. Elemental analysis for XPS reveals that the residual nitrogen content in the PNHCS is up to 6.7 wt%. It is clear that the nitrogen content in the PNHCS is much high compared with those of nitrogen-doped carbon materials (Table 1).

**Table 1** A comparison of the nitrogen content and specific capacitance of carbon materials from literature.

| Material | N content (%) | Specific capacitance (F $g^{-1}$)[a] | Ref. |
|---|---|---|---|
| N-Doped Porous Carbon Nanofibers | 7.2 | 202 (1 A $g^{-1}$) | 40 |
| N-Containing Carbons | 4.4 | 220 (0.1 A $g^{-1}$) | 41 |
| Resins derived porous carbon | 5.2 | 239.7 (0.5 A $g^{-1}$) | 23 |
| Porous N-Doped Carbon Nanotubes | 6.0 | 180 (0.5 A $g^{-1}$) | 28 |
| PNHCS | 6.7 | 213 (0.5 A $g^{-1}$) | - |

[a] Measurement conditions: three-electrode system, 6 M KOH solution.

The heteroatoms and functional groups existing in a carbon matrix can significantly change the electron/donor characteristics of the carbon electrode material. In particular, nitrogen can act as an electron donor in the lattice, resulting in a shift of the Fermi level in carbon electrodes. Nitrogen-doping can also enhance the capacitance of carbon-based materials due to a redox pseudocapacitance contribution. Previous reports suggest that during oxidation, the pyridinic-nitrogen can become either an oxidized pyridinic nitrogen or a pyrrolic nitrogen. A reversible conversion process such as this can enhances the apparent capacitance of the materials. The transformation of quaternary-N into other forms of nitrogen functionalities is extremely difficult under mild electrochemical condition.[42, 43] In addition, nitrogen-doping modifies the polarity of carbon matrixes and changes the electron distribution of the materials, which are of benefit to providing the possibility that the ions can diffuse into the micropores.[44-47] As a result, nitrogen atoms doped into carbon materials strengthen the wettability of the interface between the electrolyte and electrodes.[46, 48]

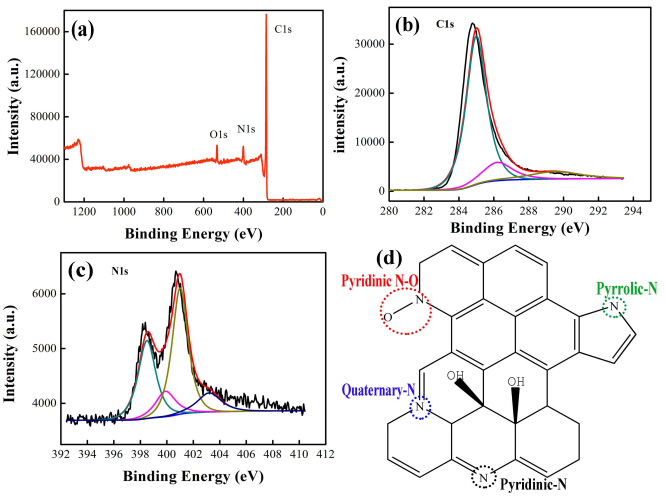


**Figure 3.** XPS spectra of the PNHCS sample: (a) survey spectrum; (b) C1s spectrum; and (c) N1s spectrum and (d) schematic representation of the different N-based functional groups detected on PNHCS by XPS.

The $N_2$ adsorption/desorption isotherms and corresponding pore size distribution curves for the PNHCS are shown in Figure 4. The nitrogen adsorption/desorption isotherms of the PNHCS can be identified as mixed IUPAC types I and IV for a microporous and mesoporous structure (Figure 4a).[49, 50] The specific surface area of the PNHCS is 213 $m^2$ $g^{-1}$ as measured by the Brunauer-Emmett-Teller (BET) method and the total pore volume is 0.24 $cm^3$ $g^{-1}$ by the Barrett-Joyner-Halenda (BJH) method. The mesopores and macropores can be observed in Figure 4a, originating from the hollow core of the PNHCS. The average pore size is 4.5 nm. The essential microporous absorption sites have diameter of 1.4 to 1.7 nm. The mesopores can be also observed ranging from 2.2 to 32 nm (Figure. 4b).

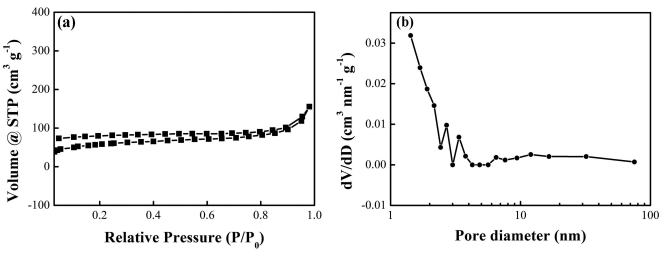


**Figure 4.** (a) $N_2$ adsorption/desorption isotherms at 77 K and (b) pore size distribution of PNHCS.

To investigate the electrochemical performance of the obtained PNHCS as an electrode material for EDLCs, they were characterized by cyclic voltammetry (CV) and galvanostatic charge/discharge measurements in a three-electrode system. The representative CV curves of the PNHCS electrode in 6 M KOH aqueous solution at different scan rates, over the range of -1.0 - 0 V (Figure 5a), are close to the capacitive curve shape expected, especially at low scan rates. With increase of scan rate, the rectangular curve shape of the sample remains, even up to 100 mV $s^{-1}$. When the scan rate increases to 200 mV $s^{-1}$, the quasi-rectangular curve shape shows only light distortion, indicating excellent capacitive

performance of PNHCS even at high current density and implying good electrochemical performance as an EDLCs electrode material.[51, 52] No pronounced reversible redox peaks were observed in the CV curves in this work, which agrees with the previous report.[23] The EDLCs behavior appears to be dominant in the capacitive performance of these materials. However, the nitrogen containing functional groups in nitrogen-enriched carbon materials can enhance the capacitance of the material by addition of redox pseudocapacitance.[28, 42, 43]

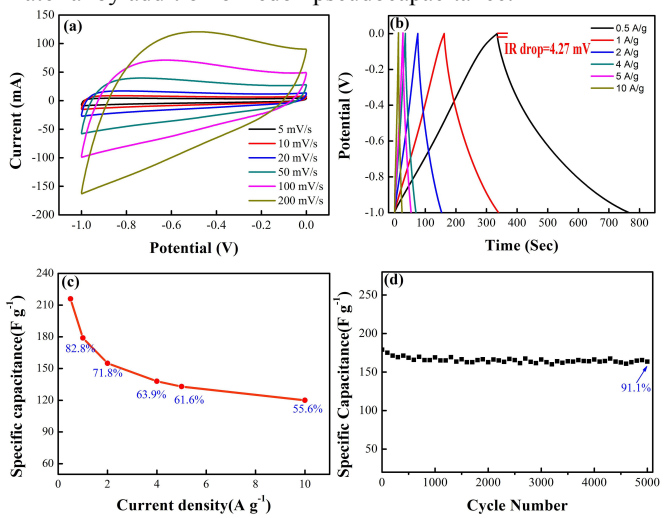


**Figure 5.** (a) CVs of the PNHCS electrode in 6 M KOH aqueous solution at different scan rates. (b) Galvanostatic charge/discharge curves of the PNHCS electrode at different current densities. (c) Plot of specific capacitances calculated from the discharge curves versus current density. (d) Cycling stability of the PNHCS with a current density of 1 A $g^{-1}$.

The galvanostatic charge/discharge curves at different current densities are present in Figure 5b. All curves show isosceles triangular shapes demonstrating a close to ideal capacitor behavior, even at current densities as high as 10 A $g^{-1}$. Noticeably, the voltage drop at the start of a discharge is 4.27 mV at a current density of 0.5 A $g^{-1}$, suggesting a very low equivalent series resistance.[53, 54] The specific capacitance can be calculated from the galvanostatic charge/discharge curves based on the following equation:

$$C = \frac{IT}{M\,\Delta V}$$

where $C$, $I$, $T$, $M$ and $\Delta V$ are the specific capacitance (F $g^{-1}$ ) of the electrode, the discharge current (A), the discharge time (s), the mass of active material and the discharge potential range (V), respectively. The PNHCS thus exhibit a capacitance as high as 213 F $g^{-1}$ at a current density of 0.5 A $g^{-1}$ which is higher than that of the nitrogen-doped polyaniline-based carbon nanotubes, ordered mesoporous carbons and graphene hydrogel under the same current density.[22, 55, 56] The specific capacitance decreases slowly with increase in charge/discharge current densities (Figure 5c). The excellent performance of such a porous carbon material is attributed to its combination of hollow spherical structure with meso-/microporous structure and the nitrogen-enriched carbon framework. This hierarchical porous structure facilitates ion transport, as well as thus contributes synergistically to the high rate performance.[53-57] To evaluate the cycle life of the PNHCS for practical applications, the change of specific capacitance versus cycle number for the PNHCS at the current density of 1 A $g^{-1}$ is presented in Figure 5d. The capacitance of PNHCS decreases by only 8.9% after 5000 cycles, indicating a good cycling stability as an EDLC electrode material.

The excellent rate performance and electrochemical stability of the PNHCS can be explained as follows. The hollow macro-structure plays a role of ion reservoir ensuring that ion depletion does not become a limiting factor at high rates. We describe this as an "ion-buffering" effect of this internal volume. The micropores of the PNHCS are favorable for enlarging the specific surface area, and mesopores offer larger channels for liquid electrolyte access and ion transport. With this unique combination of microporous and meso-/macroporous structures, it is demonstrate that the PNHCS are promising materials for supercapacitors applications.

## Conclusions

In summary, we have prepared hollow carbon spheres with hierarchical porous structure and nitrogen-doping. SPS spheres were used as the hard cores for coating a thin shell of PANI through chemical polymerization of aniline, resulting in SPS@PANI core-shell structures. After removing the SPS sphere and pyrolysis, PNHCS with uniform dimensions and complete morphology were obtained. It was demonstrated that the nitrogen doping and porous structure of the PNHCS favors the rapid diffusion of electrolyte ions, resulting in superior capacitive performance, excellent rate performance and long-term cycling stability. At a current density of 0.5 A $g^{-1}$, these PNHCS present a high specific capacitance of 213 F $g^{-1}$, and the capacitance decreases only by 44% at 10 A $g^{-1}$. The specific capacitance of the PNHCS decreases by only 8.9% after 5000 cycles at 1 A $g^{-1}$ and appears to be quite stable at that point. This indicates high chemical and strucural stability of the PNHCS material.

## Experimental

### Materials

Aniline (A.R., Shanghai Chemical Reagent Co. Ltd.) was distilled under reduced pressure. All other reagents used in our experiments were analytical reagent grade and were used without further purification.

### Synthesis of SPS spheres

Styrene (42 ml) was dissolved in distilled water (400 ml), and then stirred at room temperature for 1 h. After the addition of potassium persulfate (1 g), the solution was heated to 70 °C with vigorous stirring. The polymerization was allowed to proceed for 24 h.[26, 27] All steps were performed under nitrogen. Then the product was washed with ethanol and dried in vacuum at 60 °C for 12 h. The obtained PS powder (2 g) dissolved in

concentrated sulfuric acid (60 ml, 98%) was heated to 40 °C under vigorous stirring for 6 h. After cooling to room temperature, the SPS spheres were collected by centrifugation and washed several times with ethanol. The as-obtained SPS spheres were further dried in vacuum at 60 °C for 12 h.

### Synthesis of HPS

SPS powder (0.5 g) was dispersed in hydrochloric acid (30 ml, 1 M). Aniline monomer (0.2 ml) was then added to the above mixture. The mixture was stirred in an ice bath for 6 h. APS (0.5 g) was dissolved in hydrochloric acid (20 ml, 1 M) and was dropped into the suspension. The polymerization was carried out for 24 h by stirring slowly at 0 °C. The resulting PANI-coated SPS particles were purified by repeated centrifugation and dried in vacuum drying oven at 60 °C for 12 h. The as-obtained SPS@PANI core-shell spheres were dispersed into DMF to remove the SPS cores. Then the HPS were obtained.

### Synthesis of PNHCS

The as-prepared HPS were heated to 600 °C under nitrogen atmosphere with a heating rate of 5 °C $min^{-1}$, and kept at this temperature for 1.5 h to obtain the PNHCS.

### Characterization

Scanning electron microscopy (SEM) and transmission electron microscopy (TEM) measurements were carried out with JEOL JSM-6380LV FE-SEM and FEI TECNAI-20, respectively. Fourier transform infrared spectrometry (FT-IR) measurements were recorded on a Nicolet 750. The $N_2$ adsorption/desorption tests were determined by Brunauer-Emmett-Teller (BET) measurements using an ASAP-2010 surface area analyzer. The X-ray photoelectron spectroscopy (XPS) analysis was performed on a Perkin-Elmer PHI 550 spectrometer with Al Ka (1486.6 eV) as the X-ray source.

### Electrochemical characterization

Cyclic voltammetry (CV) and galvanostatic charge/discharge behaviors of PNHCS electrodes were investigated on a CHI 660A electrochemical workstation (Shanghai Chenhua, China) in a conventional three-electrode system with 6 M KOH aqueous solution as the electrolyte. Platinum foil and a saturated calomel electrode (SCE) were used as counter and reference electrodes. The working electrodes were prepared by mixing active material (5 mg) and polytetrafluoroethylene (PTFE) binder with a weight ratio of 85:10:5. After coating the above slurry on foamed Ni grids (1 cm×1 cm), the electrodes were dried at 60 °C for several hours before pressing under a pressure of 10 MPa.

## Acknowledgements

This work was supported by the National Natural Science Foundation of China (No. 21103091, 21173120, 51372116), National Basic Research Program of China (973 Program) (No. 2014CB239701), and Natural Science Foundation of Jiangsu Province (BK2011030), and the Foundation of Graduate Innovation Center in NUAA (kfjj20130219).

## Notes and references

[a] College of Materials Science & Engineering, Nanjing University of Aeronautics and Astronautics, Nanjing, 210016 (P.R. China)
Fax: +86-025-52112918; Tel: +86-025-52112626
E-mail: dh_msc@nuaa.edu.cn
[b] Australian Centre for Electromaterials Science, Monash University, Clayton Victoria 3800 (Australia)
Fax: +61-3-99054597; Tel: +61-3- 99054540
E-mail: Douglas.MacFarlane@monash.edu

1. N. S. Choi, Z. Chen, S. A. Freunberger, X. Ji, Y. K. Sun, K. Amine, G. Yushin, L. F. Nazar, J. Cho and P. G. Bruce, *Angew. Chem. Int. Ed.*, 2012, **51**, 9994-10024.
2. X. Lai, J. E. Halpert and D. Wang, *Energy Environ. Sci.*, 2012, **5**, 5604-5618.
3. Y. Zhai, Y. Dou, D. Zhao, P. F. Fulvio, R. T. Mayes and S. Dai, *Adv. Mater.*, 2011, **23**, 4828-4850.
4. C. Liu, F. Li, L. P. Ma and H. M. Cheng, *Adv. Mater.*, 2011, **22**, 28-62.
5. W. Fan, C. Zhang, W. W. Tjiu, K. P. Pramoda, C. He and T. Liu, *ACS Appl. Mater. Interfaces*, 2013, **5**, 3382-3391.
6. P. Liu, M. Verbrugge and S. Soukiazian, *J. Power Sources*, 2006, **156**, 712-718.
7. J. Gamby, P.L. Taberna, P. Simon, J.F. Fauvarque, M. Chesneau, *J. Power Sources*, 2001, **101**, 109-116.
8. L. Chen, C. Yuan, H. Dou, B. Gao, S. Chen and X. Zhang, *Electrochim. Acta*, 2009, **54**, 2335-2341.
9. K. H. An, W. S. Kim, Y. S. Park, J.M. Moon, D. J. Bae, S. C. Lim, Y. S. Lee and Y. H. Lee, *Adv. Funct. Mater.*, 2001, **11**, 387-392.
10. Y. Sun and G. Shi, *J. Polym. Sci. Part B: Polym. Phys.*, 2013, **51**, 231-253.
11. X. W. Yang, C. Cheng, Y. F. Wang, L. Qiu and D. Li, *Science*, 2013, **341**, 534-537.
12. Y. Zhao, C. Hu, Y. Hu, H. Cheng, G. Shi and L. Qu, *Angew. Chem. Int. Ed.*, 2012, **124**, 11533-11537.
13. J. Biener, M. Stadermann, M. Suss, M. A. Worsley, M. M. Biener, K. A. Rosea and T. F. Baumanna, *Energy Environ. Sci.*, 2011, **4**, 656-667.
14. M. X. Liu, L. H. Gan, W Xiong, Z. J. Xu, D. Z. Zhu and L. W. Chen, *J. Mater. Chem. A*, 2014, doi: 10.1039/C3TA14445C.
15. J. S. Qian, M. X. Liu, L. H. Gan, P. K. Tripathi, D. Z. Zhu, Z. J. Xu, Z. X. Hao, L. W. Chen and D. S. Wright, *Chem. Commun.*, 2013, **49**, 3043-3045.
16. X. M. Ma, M. X. Liu, L. H. Gan, Y. H. Zhao, L. W. Chen, *J. Solid State Electr.*, 2013, **17**, 2293-2301.
17. F. W. Ma, H. Zhao, L. P. Sun, Q. Li, L. H. Huo, T. Xia, S. Gao, G. S. Pang, Z. Shi and S. H. Feng, *J. Mater. Chem.*, 2012, **22**, 13464-13468.
18. Y. H. Zhao , M. X. Liu, L. H. Gan, X. M. Ma, D. Z. Zhu, Z. J. Xu and L. W. Chen, *Energy Fuels*, 2013, doi: 10.1021/ef402070j.
19. W. Xiong, M. X. Liu, L. H. Gan, Y. K. Lv, Z. J. Xu, Z. X. Hao, L. W. Chen, *Colloid Surface A*, 2012, **411**, 34-39.

20. L. Qie, W. M. Chen, Z. H. Wang, Q. G. Shao, X. Li, L. X. Yuan, X. L. Hu, W. X. Zhang and Y. H. Huang, *Adv. Mater.*, 2012, **24**, 2047-2050.
21. H. G. Wang, Z. Wu , F. L. Meng , D. L. Ma , X. L. Huang , L. M. Wang and X. B. Zhang, *ChemSusChem*, 2013, **6**, 56-60.
22. M. M. Yang, B. Cheng, H. H. Song and X. H. Chen, *Electrochim. Acta*, 2010, **55**, 7021-7027.
23. X. Y. Chen, C. Chen, Z. J. Zhang, D. H. Xie and X. Deng, *Ind. Eng. Chem. Res.*, 2013, **52**, 10181-10188.
24. J. J. Langer and S. Golczak, *Polym. Degrad. Stab.*, 2007, **92**, 330-334.
25. C. Wu, X. Wang, B. Ju, L. Jiang, H. Wu, Q. Zhao and L. Yi, *J. Power Sources*, 2013, **227**, 1-7.
26. D. S. Yuan, T. X. Zhou, S. L. Zhou, W. J. Zou, S. S. Mo and N. N. Xia, *Electrochem. Commun.*, 2011, **13**, 242-246.
27. S. Mentus, G. Ćirić-Marjanović, M. Trchová and J. Stejskal, *Nanotech.*, 2009, **20**, 245601.
28. G. Y. Xu, B. Ding, P. Nie, L. F. Shen, J. Wang and X. G. Zhang, *Chem. Eur. J.*, 2013, **19**, 12306-12312.
29. B. You, J. Yang, Y. Sun and Q. Su, *Chem. Commun.*, 2011, **47**, 12364-12366.
30. Z. B. Lei, Z. W. Chen and X. S. Zhao, *J. Phys. Chem. C*, 2010, **114**, 19867-19874.
31. R. Silva, D. Voiry, M. Chhowalla and T. Asefa, *J. Am. Chem. Soc.*, 2013, **135**, 7823-7826.
32. A. H. Lu, T. Sun, W. C. Li, Q. Sun, F. Han, D. H. Liu and Y. Guo, *Angew. Chem. Int. Ed.*, 2011, **50**, 11765-11768.
33. Y. Yang, Y. Chu, F. Yang and Y. Zhang, *Mater. Chem. Phys.*, 2005, **92**, 164-171.
34. X. Y. Dai, X. Zhang, Y. F. Meng and P. K. Shen, *New Carbon Mater.*, 2011, **26**, 389-395.
35. L. J. Pan, G. H. Yu, D. Y. Zhai, H. R. Lee, W. T. Zhao, N. Liu, H. L. Wang, B. Tee, Y. Shi, Y. Cui and Z. N. Bao, *PNAS*, 2012, **109**, 9287-9292.
36. M. Zhang, L. L. Bai, W. H. Shang, W. J. Xie, H. Ma, Y. Y. Fu, D. C. Fang, H. Sun, L. Z. Fan, M. Han, C. M. Liu and S. H. Yang, *J. Mater. Chem.*, 2012, **22**, 7461-7467.
37. S. Y. Gao, H. Fan, Y. L. Chen, L. Li, Y. Bando and D. Golberg, *Nano Energy*, 2013, **2**, 1261-1270.
38. V. Datsyuk, M. Kalyva, K. Papagelis, J. Parthenios, D. Tasis, A. Siokou, I. Kallitsis and C. Galiotis, *Carbon*, 2008, **46**, 833-840.
39. M. Sevilla, P. Valle-Vigón and A. B. Fuertes, *Adv. Funct. Mater.*, 2011, **21**, 2781-2787.
40. L. F. Chen, X. D. Zhang, H. W. Liang, M. G. Kong, Q. F. Guan, P. Chen, Z. Y. Wu and S. H. Yu, *ACS Nano*, 2012, **6**, 7092-7102.
41. L. Zhao, L. Z. Fan, M. Q. Zhou, H. Guan, S. Y. Qiao, M. Antonietti and M. M. Titirici, *Adv. Mater.*, 2010, **22**, 5202-5206.
42. D. W. Wang, F. Li, L. C. Yin, X. Lu, Z. G. Chen, I. R. Gentle, G. Q. Lu and H. M. Cheng, *Chem. Eur. J.*, 2012, **18**, 5345-5351.
43. H. M. Jeong, J. W. Lee, W. H. Shin, Y. J. Choi, H. J. Shin, J. K. Kang and J. W. Choi, *Nano Lett.*, 2011, **11**, 2472-2477.
44. H. L. Guo, Q. M. Gao, *J. Power Sources*, 2009, **186**, 551-556.
45. W. J. Qian, F. X. Sun, Y. H. Xu, L. H. Qiu, C. H. Liu, S. D. Wang and F. Yan, *Energy Environ. Sci.*, 2014, **7**, 379-368.
46. W. Li, D. Chen, Z. Li, Y. Shi, Y. Wan, G. Wang, Z. Jiang and D. Zhao, *Carbon*, 2007, **45**, 1757-1763.
47. L. Hao, X. L. Li and L. J. Zhi, *Adv. Mater.*, 2013, **25**, 3899-3904.
48. W. Li, D. Chen, Z. Li, Y. Shi, Y. Wan, J. Huang, J. Yang, D. Zhao and Z. Jiang, *Electrochem. Commun.*, 2007, **9**, 569-573.
49. S. H. Chung and A. Manthiram, *J. Mater. Chem. A*, 2013, **1**, 9590-9596.
50. A. P. Katsoulidis, S. M. Dyar, R. Carmieli, C. D. Malliakas, M. R. Wasielewski and M. G. Kanatzidis, *J. Mater. Chem. A*, 2013, **1**, 10465-10473.
51. F. Xu, R. Cai, Q. Zeng, C. Zou, D. Wu, F. Li, X. Lu, Y. Liang and R. Fu, *J. Mater. Chem.*, 2011, **21**, 1970-1976.
52. L. F. Chen, Z. H. Huang, H. W. Liang, W. T. Yao, Z. Y. Yu and S. H. Yu, *Energy Environ. Sci.*, 2013, **6**, 3331-3338.
53. D. C. Guo, J. Mi, G. P. Hao, W. Dong, G. Xiong, W. C. Li and A. H. Lu, *Energy Environ. Sci.*, 2013, **6**, 652-659.
54. D. W. Wang, F. Li, M. Liu, G. Q. Lu and H. M. Cheng, *J. Phys. Chem. C*, 2008, **112**, 9950-9955.
55. J. X. Wang, C. F. Xue, Y. Y. Lv, F. Zhang, B. Tu, D. Y. Zhao, *Carbon*, 2011, **49**, 4580-4588.
56. Y. X. Xu, K. X. Sheng, C. Li and G. Q. Shi, *ACS Nano*, 2010, **4**, 4324-4330.
57. Y. Mun, C. Jo, T. Hyeon, J. Lee, K. S. Ha, K. W. Jun, S. H. Lee, S. W. Hong, H. I. Lee, S. Yoon and J. Lee, *Carbon*, 2013, **64**, 391-402.



 